INSTITUTE OF PHYSICS PUBLISHING PHYSICAL BIOLOGY
Phys. Biol. **2** (2005) 60–72 doi:10.1088/1478-3967/2/1/008

# Tracking single particles: a user-friendly quantitative evaluation

**Brian C Carter**[1], **George T Shubeita**[2] **and Steven P Gross**[1,2]

[1] Department of Physics and Astronomy, University of California Irvine, Irvine, CA 92612, USA
[2] Department of Developmental and Cell Biology, University of California Irvine, Irvine, CA92612, USA

E-mail: sgross@uci.edu

Received 6 January 2005
Accepted for publication 28 February 2005
Published 21 March 2005
Online at stacks.iop.org/PhysBio/2/60

**Abstract**
As our knowledge of biological processes advances, we are increasingly aware that cells actively position sub-cellular organelles and other constituents to control a wide range of biological processes. Many studies quantify the position and motion of, for example, fluorescently labeled proteins, protein aggregates, mRNA particles or virus particles. Both differential interference contrast (DIC) and fluorescence microscopy can visualize vesicles, nuclei or other small organelles moving inside cells. While such studies are increasingly important, there has been no complete analysis of the different tracking methods in use, especially from the practical point of view. Here we investigate these methods and clarify how well different algorithms work and also which factors play a role in assessing how accurately the position of an object can be determined. Specifically, we consider how ultimate performance is affected by magnification, by camera type (analog versus digital), by recording medium (VHS and SVHS tape versus direct tracking from camera), by image compression, by type of imaging used (fluorescence versus DIC images) and by a variety of sources of noise. We show that most methods are capable of nanometer scale accuracy under realistic conditions; tracking accuracy decreases with increasing noise. Surprisingly, accuracy is found to be insensitive to the numerical aperture, but, as expected, it scales with magnification, with higher magnification yielding improved accuracy (within limits of signal-to-noise). When noise is present at reasonable levels, the effect of image compression is in most cases small. Finally, we provide a free, robust implementation of a tracking algorithm that is easily downloaded and installed.

S This article has associated online supplementary data files

**Abbreviation list**

| | |
|---|---|
| *BPD* | Beam position detector using quadrant photodiode |
| *CCD* | Charge coupled device |
| *COR* | Correlation (normalized correlation coefficient) |
| *DIC* | Differential interference contrast |
| *ISeeCM* | ISee method using correlation with a centroid interpolation |
| *ISeePSF* | ISee method using correlation with a parabolic surface fit interpolation |
| *ISeeACM* | ISee method using correlation with an adaptive centroid interpolation |
| *JPEG* | Joint photographic experts group |
| *LVCent* | LabVIEW method using centroid to determine object center |
| *LVCOR* | LabVIEW correlation-based method with centroid interpolation |
| *LVPara* | LabVIEW correlation-based method with parabolic interpolation |
| *LVPSF* | LabVIEW correlation-based method with parabolic surface fit interpolation |
| *MetaThresh1* | MetaMorph centroid method with automatic threshold for light objects |
| *MetaThresh2* | MetaMorph centroid method with manual threshold |

  

| | |
|---|---|
| *MetaTM* | MetaMorph method which matches template by convolution |
| *MPEG* | Motion picture experts group |
| *NA* | Numerical aperture |
| *OpenCV* | Open computer vision |
| *S/N* | Signal-to-noise ratio |
| *SAD* | Sum-absolute difference |
| *SEM* | Standard error of the mean |

## Introduction

Advances in understanding the link between signaling pathways and molecular motor-based transport [1–3], in linking neurodegenerative diseases to active transport [4, 5], in investigating how the cytoplasm is appropriately partitioned during cell division [6] and in understanding protein aggregation, destruction and prion diseases [7, 8], have all highlighted the need for accurate determination of the position and motion of sub-cellular organelles. Nanometer-scale particle tracking has many uses, including determination of diffusion constants of proteins in cell membranes [9], step displacements of beads attached to molecular motors [10, 11] and displacement of actin fibers or microtubules driven by molecular motors [12]. Luckily, the combination of new fluorescent technologies that label specific proteins or sub-cellular structures and tremendously increased computer speed have made it possible to gather large quantities of high-quality data reflecting the position versus time of many such objects. Here we review methods for tracking nanometer-scale objects, and evaluate factors that can alter the ultimate accuracy of determination of a particle's position. For the non-specialist, we provide specific suggestions for robust ways to achieve results with nanometer-level accuracy.

Methods used for tracking algorithms include finding the center of mass (centroid) of the object [9, 13], fitting a Gaussian curve to the object [14–17], cross-correlation and its derivatives (COR) [10, 18, 19] and sum-absolute difference (SAD) [20]. However, methods such as COR and SAD do not give sub-pixel position on their own. Instead they create a 'correlation image' showing regions of high similarity between a template image and the current image. A method of interpolating the nearest sub-pixel position of this 'correlation object' is then necessary. The types of interpolation that have been used include parabolic, cosinusoidal, and Gaussian [21] fitting and centroid calculation [10]. Currently, the method of choice for tracking in many laboratories [18, 19] is to apply a COR-based algorithm, followed by centroid interpolation to give sub-pixel position. Such a method was previously described [10] and is used in some form in the commercial programs described below.

In the methods of particle tracking examined here, tracking begins with the selection of a region of interest. Then, in each image, the chosen method of locating the particle's center is applied and this center position is used to reposition the area of interest for the next image acquired. The methods for locating the center of a particle examined here can be broken down into two broad groups: pure centroid-based methods and correlation-based methods.

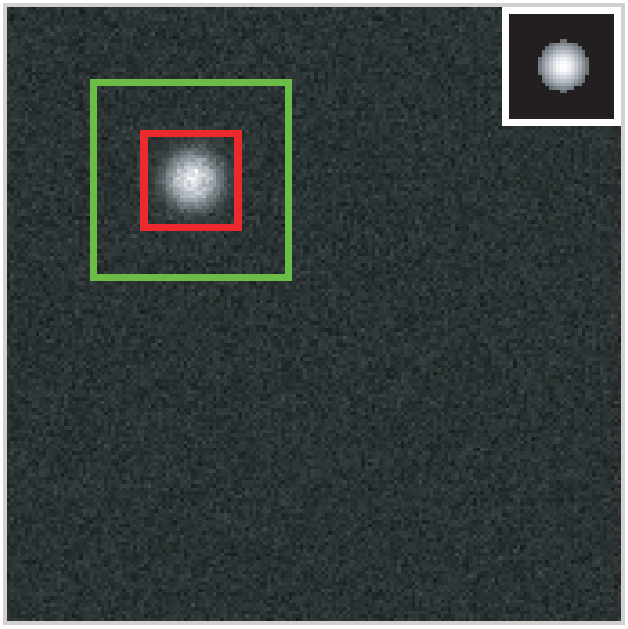

**Figure 1.** A sample image used during testing of the different tracking algorithms. The inner square is the template chosen, the outer square is the search area. Inset: a sample correlation image taken during execution of the LabVIEW COR (LVCOR) tracking algorithm. The template size is 26 × 26 pixels and the search region is 54 × 54 pixels which results in a square correlation image with (54–26) + 1 pixels on each side.

For methods based solely on centroid calculation, a search region is placed as tightly around the object of interest as possible (given how far the particle can move between frames). Before the centroid is calculated, a threshold operation is performed to remove as much background noise as possible without losing the edge of the object. Then the center of mass is calculated and used to re-center the search region for the next frame.

Tracking a particle in an image sequence using a correlation method requires choosing a template image to be searched for in subsequent images. The algorithm overlays and calculates a correlation with this template image for each point within the selected search region, creating a correlation image where high brightness indicates high correlation. This is illustrated in figure 1. A threshold is applied to the correlation image to remove the background and the center of the correlation image is then found using an interpolation method (in this paper, parabolic, centroid, or parabolic surface fit).

Depending on the exact implementation of particle tracking used, investigators typically propose that an accuracy of ∼10 nm or better can be achieved [10, 18, 22]. When magnification and the physical size of the pixels in the CCD chip of the camera are considered, the image pixel size is typically between 30 nm/pixel and 150 nm/pixel (see e.g. [22]). Thus, to achieve an accuracy of 10 nm corresponds to locating the center of the object to somewhere between 1/3 and 1/15th of a pixel. The term 'accuracy' used throughout this paper should not be confused with optical resolution, namely,

the smallest distance between two objects that a microscope can distinguish. The latter is limited in the far field by the wavelength of light used for imaging. However, in an image where a particle is well separated from any other particles, determination of its position is not limited by the wavelength and has no obvious theoretical limitation. The term accuracy thus reflects the uncertainty with which a method determines the position of this single particle being tracked.

Past work by Cheezum *et al* [21] quantitatively compared four methods of tracking: Gaussian, centroid, COR and SAD, using computer- generated fluorescence images ranging in size from point sources to several microns in diameter. All four methods failed as the noise in the sample increased, and in particular as the signal-to-noise approached 4. Both the COR and SAD algorithms were tested with cosinusoidal, Gaussian and parabolic interpolation to achieve sub-pixel accuracy. For objects on the order of size of the wavelength of light and larger, direct Gaussian fitting is inappropriate, so only the centroid, SAD and COR methods were tested. It was found that all three of these methods were subject to some level of pixel bias error, i.e. the method displays a 'preference' for certain positions within a pixel. While COR followed by a centroid interpolation is an often-used method [10, 18, 19], it was not tested.

Cheezum *et al*'s study was useful but failed to consider many important practical issues that we shall address here. First, the commonly used 'COR followed by centroid' option needs to be evaluated. Second, for a non-technical user, how well do the commercial, 'off-the-shelf' options work? Here, we compare a number of algorithms that we implement in LabVIEW with two 'off-the-shelf' options: ISee and MetaMorph. Third, a number of choices can be made in the details of the microscopy. Which ones are important, and to what extent? Finally, there could be many real world sources of 'noise'. What are some of the most significant sources, and what is their effect on tracking?

## Materials and methods

Two commercial tracking programs (ISee and MetaMorph)[3,4] were compared with four tracking programs written in LabVIEW[5]. The specific tracking methods used in ISee were 'correlation coefficient' combined with either 'center of mass' (ISeeCM), 'parabolic surface fit' (ISeePSF) or 'adaptive center of mass' (ISeeACM) these being methods used to calculate the center position of the object in the correlation image. Under MetaMorph, track objects 'threshold image' (a centroid-based method) was used with two different kinds of thresholding 'light object' (MetaThresh1) and manual (MetaThresh2). In MetaMorph, we also used track objects 'template match' (MetaTM) (both with and without derivative active). Template match with derivative active did not consistently track, so it was excluded from further consideration. In LabVIEW, the four methods tested were 'normalized correlation coefficient' (implemented through OpenCV[6] code, same correlation method as ISee) followed by centroid (LVCOR) (same as 'center of mass'), parabolic interpolation (LVPara) or parabolic surface fit (LVPSF), and centroid with an applied threshold (LVCent). The LabView method accompanying this paper as a free download is the correlation-based method with centroid calculation referred to as LVCOR throughout the manuscript. It is available for download on the Gross-lab website: http://bioweb.bio.uci.edu/sgross/.

### *Centroid-based methods*

Pure centroid-based methods apply a threshold to the image and then compute the energy center of the region of interest. The energy center of the grayscale image of width $w$ and height $h$ is calculated as follows:

$$\overline{x} = \frac{\sum_{x=0}^{w}\sum_{y=0}^{h} xI(x,y)}{\sum_{x=0}^{w}\sum_{y=0}^{h} I(x,y)}, \qquad \overline{y} = \frac{\sum_{x=0}^{w}\sum_{y=0}^{h} yI(x,y)}{\sum_{x=0}^{w}\sum_{y=0}^{h} I(x,y)} \tag{1}$$

where $x$ is the current $x$ position, $y$ is the current $y$ position, and $I(x, y)$ is the intensity of the image at point $(x, y)$. Various methods may be used to select an appropriate threshold. An appropriate threshold is one that minimizes the appearance of noise while retaining as much of the object (and its shape) as possible (see supplementary figure III available from stacks.iop.org/PhysBio/2/60). Two programs which use this method were tested, a custom LabVIEW program (LVCent) and MetaMorph centroid with auto threshold light on (MetaThresh1) and MetaMorph centroid with the threshold manually set (MetaThresh2).

In LVCent the centroid is calculated using the LabVIEW IMAQ centroid function, taking into account pixels with values above the threshold. The position of the search region is then updated to place the coordinates of the centroid at the center of the search region. The threshold value is determined by use of IMAQ Auto B threshold that computes the optimal threshold value of an image based on the requested statistical method (in this case inter-class variance). Thresholding is then implemented with IMAQ threshold.

In the MetaThresh1 method, a threshold isolating bright objects is applied and a center-of-mass calculation is performed on the search region in each image. No details are given on how the threshold level is chosen.

In the MetaThresh2 method, a threshold is chosen manually so that the background is minimized without undue changes to the shape of the object being tracked. A center-of-mass calculation is then performed on the search region in each image.

### *Correlation-based methods*

Many methods make use of a correlation algorithm to locate regions within an image that have high identity with a sample

[3] ISee version 5.1.2. ISee is available from ISee imaging systems, http://www.iseeimaging.com/.

[4] MetaMorph (version 6.1 r5 used for this paper) is available from Universal Imaging Corporation, http://www.universal-imaging.com/index.cfm.

[5] LabVIEW version 6.1. LabVIEW is available from National Instruments, http://www.ni.com/.

[6] OpenCV (Open Computer Vision version beta 3) is available through SourceForge.net, http://sourceforge.net/projects/opencvlibrary/.

image, known as the template (figure 1). Put simply, the template image is overlayed and compared to the image of interest and moved over the image of interest one pixel at a time, with each location being scored for its similarity to the template image. This set of similarity scores build up a correlation image. The correlation image has the advantage of low noise, since many points are compared to many other points to create it. The method ISee used, and which we used for our LabVIEW programs, is the normalized correlation coefficient, which is calculated as follows:

$$R(x, y) = \frac{\sum_{x'}^{w} \sum_{y'}^{h} (T(x', y') - \overline{T})(I(x + x', y + y') - \overline{I})}{\sqrt{\sum_{x'}^{w} \sum_{y'}^{h} (T(x', y') - \overline{T})^2 \sum_{x'}^{w} \sum_{y'}^{h} (I(x + x', y + y') - \overline{I})^2}} \quad (2)$$

where $R$ is the correlation image, $w$ is the width of the template, $h$ is the height of the template, $T$ is the template image, $I$ is the search area image, $\overline{T}$ is the mean pixel value of the template, $\overline{I}$ is the mean pixel value of the image within the current area ($x'$, $y'$ to $x' + w$, $y' + h$), $(x, y)$ and $(x + x', y + y')$ are the pixel positions in the respective images (template and search area).

This gives a result for each point between $-1$ and 1. Negative values indicate negative correlation and are excluded. The brightness of the correlation matrix is scaled from 0 to 10 000 in ISee and from 0 to 30 000 in LabVIEW. Correlation methods on their own give a correlation image ($R(x, y)$). By selecting the brightest point you can get an estimate to one pixel of the center of the object, but sub-pixel accuracy is usually desired since one pixel is usually tens of nanometers across. To achieve sub-pixel accuracy, one of the following methods was applied:

*Parabolic interpolation.* The brightest pixel in the correlation image is identified and a parabolic fit is performed in $x$ and $y$ using one point to either side as described in Cheezum *et al* [21] (equations (12), (13), (14)). This method is used in the LabVIEW parabolic fit (LVPara) program.

*Centroid (center of mass).* The energy center of the grayscale correlation image is computed as in equation (1). This is done after the application of a threshold to remove the background correlation. This method is used by LabVIEW correlation/centroid (center of mass) (LVCOR) and ISee center of mass (ISeeCM). LVCOR uses IMAQ[7] centroid which computes the energy center of the grayscale correlation image.

ISee adaptive center of mass (ISeeACM) uses a variation of this procedure where it first performs a feature extraction (no details provided in the NanoTrack manual) in the correlation matrix to remove any correlation with other objects in the scan area and then computes the center of mass as in ISeeCM.

The LVCOR method together with user instructions is available for download on the Gross-lab website: http://bioweb.bio.uci.edu/sgross/. When you download this program, please email us so we can send future updates or program corrections. As a condition of use, you must acknowledge the use of the program in any resulting manuscript, and cite this manuscript. Such cites will help track usage, allowing us to justify to the NIH (National Institute of Health) the utility of developing future free software, including updates and extensions to the currently distributed tracking program.

[7] IMAQ-Vision (IMAQ-Vision Builder 6) is a package of programs available from National Instruments which are used for machine vision applications.

*Parabolic surface fit (PSF).* This method fits the correlation image to a two-dimensional parabolic function to compute the position of the object. This method is used by Labview parabolic surface fit (LVPSF) and by ISee parabolic surface fit (ISeePSF). The NanoTrack Manual for ISee does not give details on the algorithm used to find the 2d parabolic surface fit. In the LVPSF method a grid of points either $6 \times 6$ (even) or $7 \times 7$ (odd) centered on the brightest pixel in the correlation matrix is fit by a parabolic surface and the sub-pixel center coordinates are extracted from the equation of the parabolic surface. The equation fit is of the form, $v = A + Bx + Cy + Dx^2 + Ey^2$ solved by the method of multiple linear regression to give the least-squares fit.

*Template match (TM).* A method which performs a convolution between the first image and the current image. This method is used only by MetaMorph template match (MetaTM). Details on what exactly this method does are not available in the manual, but is likely correlation related.

*Comparison of methods*

Tracking methods were compared using several standards: fixed bead moved in $x$ and imaged with a differential interference contrast (DIC) microscope, simulated fluorescent bead moved in $x$ and $y$ with and without noise added (the noise varying in strength), simulated DIC bead moved in $x$ and $y$ with and without noise and simulated fluorescence images compressed by different degrees. A measure of the deviation of the measured position from the expected one was then calculated as described in the results section. In cases where an absolute position reference was unavailable (e.g. for DIC images where the stage was moved to create bead motion) methods were compared by taking the difference between the track and the best-fit line to the track. When compared on sample images where the position was known this method was found to have only small deviations. Artificial image stacks are, unless otherwise stated, 550 frames long with a displacement of 1/11th of a pixel between frames.

*Generation of fluorescence test images.* Pseudo-fluorescence images were generated using the method described in Cheezum *et al* [21] both with and without noise. Briefly, a solid white object is first created in a matrix 11 times larger than the desired final matrix to allow sub-pixel positioning of the object. The solid object is then transformed by a point-spread function which incorporates information on the magnification and the numerical aperture of the simulated microscope. The matrix thus obtained is subsequently integrated to get the final image size. Noise, assumed to be shot noise (Poisson), is

then added and the pixel values scaled to a 256 grayscale to match the images taken by the microscope system. Images generated programmatically were saved as TIFF files and were then converted to other formats as desired. Conversion to compressed forms was accomplished using QuickTime[8]. Compressed movies were decompressed to TIFF files so that all tracking methods would be tracking identical image sequences. This procedure preserves artifacts produced by compression and may introduce a small error of its own, but since this is present for all methods it is inconsequential for our investigation.

*Generation of DIC test images.* Pseudo-DIC images were generated using a variant of the method described above. The major difference is the use of an object that simulates the optical properties of a DIC image, generated by the method described by Young *et al* [23] instead of a solid object before transformation by a point-spread function. After passing through the point-spread function the final image reproduces many of the properties of true DIC images, such as the appearance of shadowed and light regions and the presence of a symmetry axis.

*Recording of real analog/digital DIC images.* Analog DIC images were generated by moving a piezoelectric stage smoothly with a bead fixed to the coverslip in the field of view. As the stage moved, image sequences were recorded to VHS cassette or SVHS cassette with time-base corrector (JVC SR-V10U). The moving bead was either tracked directly in real time or from cassette (LabVIEW only) or digitized as QuickTime JPEG A using the media recorder on a Silicon Graphics (O2) computer (IRIX Release 6.5), converted to a TIFF stack by Apple QuickTime (6.5.1), and then tracked using LabVIEW, ISee and MetaMorph.

Digital DIC images were generated by moving the piezoelectric stage as described above, but were instead recorded using a Basler A311f firewire camera (Basler BCAM version 1.8.0034) and StreamPix software (NorPix, version 3.13.0) and saved as an uncompressed AVI on a RAID 0 array on a Dell Dimension 8200 computer. The AVI was converted to QuickTime JPEG A using QuickTime and then converted to a TIFF stack for tracking using LabVIEW, ISee and MetaMorph.

*Calculation of signal-to-noise ratio (S/N)*

As the signal-to-noise ratio of the tracked object can determine how accurately it can be followed, in some cases this ratio must be calculated. The signal-to-noise ratio (S/N) is calculated as [24]

$$\frac{S}{N} \approx \frac{C_{\text{on}} - n\langle x_{\text{back}}\rangle}{\sqrt{(C_{\text{on}} - n\langle x_{\text{back}}\rangle)/G + n\sigma^2_{\text{back}} + n\sigma^2_{\text{back}}/p}} \tag{3}$$

where $C_{\text{on}}$ is the total pixel value of a box centered on the object, $n$ is the number of points in this box, $x_{\text{back}}$ is the mean background from a box not centered on the object, $p$ is the size of this second box and $G$ is the gain of the system (effectively, the number of photoelectrons per pixel brightness level, necessary as the camera output is read to be between 0 and 255). For the simulated images the gain is known to be either 1 (S/N 8.4 and 13.9), 2 (S/N 21.3) or 4 (S/N 29.5). Usually for images from a camera the gain is not known. It can be estimated, however, from the standard deviation of the background of an image (assuming a Poisson distribution for the noise). An example is provided below using a real DIC image (supplementary figure I available from stacks.iop.org/PhysBio/2/60). The S/N values used in this paper are maximum S/N within the object calculated with $n = 1$ (calculate S/N for every pixel in the image) and $p = 400$ (a $20 \times 20$ background area is used to calculate the $\sigma$ used everywhere).

To estimate the gain, first calculate the mean and standard deviation of the pixel values in a region of the background. The noise (standard deviation, $\sigma$) of a poisson process should be $\sqrt{N}$, where $N$ is the number of photoelectrons giving rise to the signal. If the gain is 1, then $B = \sigma^2 = N$ where $B$ is the mean background pixel value. If the gain is not one, then $B \neq \sigma^2$ and the ratio gives the gain, thus $G = \frac{B}{\sigma^2}$. To test this, the maximum S/N was calculated for cases where $G$ was already known. The results were as follows: For S/N 8.4 (gain known to be 1), $G$ was found to be 0.99; for S/N 13.9 (gain known to be 1), $G = 0.97$; for S/N 21.3 (gain known to be 2), $G = 2.03$; for S/N 29.5 (gain known to be 4) $G = 3.84$. All of the calculated values are within 5% of the values chosen when generating test images, which validates the use of this approach as an estimate of the true gain in cases when the gain is unknown. A more detailed method requiring more images may be found at the Photometrics website [25] and references therein.

## Results and discussion

*Overview*

Tracking accuracy can be influenced by three general classes of effects: details of the microscopy, the effect of a variety of sources of 'noise' and the specific tracking algorithm (and its implementation). The details of the different tracking algorithms tested, and their implementations, were given in the materials and methods section but the actual evaluation of their performance is presented below. Before going into the experimental details, we shall briefly summarize the different sources of noise, and the general features of microscopy that could impact tracking performance.

There are many factors that contribute to the effective noise within an image before tracking occurs. Among the most significant are: the shot noise in the camera's CCD, jitter from mechanical and electronic noise in the device used for recording (VCR, typically), analog-to-digital conversion artifacts occurring when the cassette is digitized for tracking, and digital compression, which is often used to make the file size manageable when digitized images are stored on the hard drive. Additionally, analog camera interlacing results

[8] Both QuickTime (version 6.5) and Windows Media Player will compress to many formats but use the extension .mov or .wmv. The extension does not necessarily tell you the codec (compression method) used.

in moving objects displaying a serrated edge. These sources of noise within the image can each have an effect on how accurately an object can be tracked. Moreover, a number of the aspects of the microscopy employed can in principle influence tracking performance. These include fluorescence versus DIC microscopy, magnification and numerical aperture. Below, we evaluate the contribution of each of these factors individually.

To compare the different tracking methods and the effects of the various manipulations of the images, we quantified the accuracy of the tracking method using the mean radial error. This is determined by taking the difference between the measured and expected $x$ and $y$ positions at every frame, and then computing the radial displacement as $r = \sqrt{\Delta x^2 + \Delta y^2}$. The mean is then determined simply as $\Sigma r/N$ where $N$ is the number of frames examined. Thus, a smaller value of the mean radial error reflects higher accuracy. Constant systematic shifts in the measured $x$ and $y$ positions could lead to an overestimate of the mean radial error. Hence, the latter was calculated after aligning the measured and expected tracks in a way that minimizes the total error.

With this brief overview complete, we now turn to our experiments testing the impact of each of these factors.

*Sources of noise and noise effects*

Shot noise results from variations in the number of photons striking the detector at any given time. It is a Poisson process resulting in noise with an amplitude of $\sqrt{N}$, when $N$ is the number of photoelectrons collected at the surface. This sort of noise is unavoidable in an optical system and becomes more significant at low light levels. Noise can also result from the mechanical jitter from recording to video cassette and the electronics of the VCR. Any traditional recording method requires analog-to-digital conversion in order to track on a computer, and this conversion results in pixel jitter and the addition of further electronic noise. Once an image is digitized, it may be digitally compressed to take up less hard drive space. Most compression algorithms introduce artifacts, resulting in possible distortion or noise in the image. In the following paragraphs these issues are addressed.

*Signal-to-noise effects.* Cheezum *et al* demonstrated that below a S/N of about 4 the response of all tracking algorithms they tested became essentially random. Experimental images are rarely free of noise and the performance of the different tracking algorithms is expected to be sensitive to such noise. We measured the accuracy of our test methods versus S/N and found a sharp fall-off in accuracy beginning around a signal to noise of 9 (figure 2). For a reasonable-quality image we would expect a S/N value of 10 or above; over this range most methods performed quite nicely, with the exception of MetaTM (over the entire range). Figure 3 shows typical histograms of the radial error. The distribution around the mean is relatively large and grows with the mean. Our tests suggest that accuracy for determination of a particle position in a DIC image is approximately the same as for a particle in a fluorescence image given certain caveats (see below).

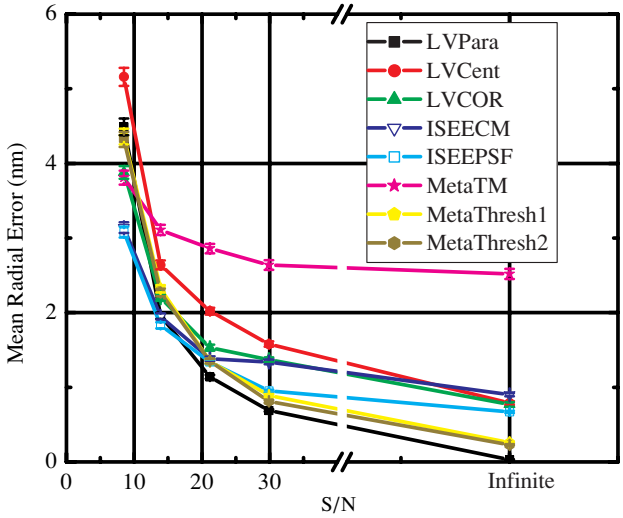


**Figure 2.** The accuracy of the different tracking methods as a function of S/N. MetaThresh1 and 2 do the best from S/N 29.9 to S/N 13.9. At S/N 8.5 the ISee methods achieve the best results, while the accuracy of LabVIEW Cent falls to an unacceptable level. The magnification was 33 nm/pixel. Error bars represent the SEM for 550 measurements.

*Effects due to VCR recording.* To test the effect of video tape recording on the accuracy of position determination, a 450 nm bead stuck to a microscope coverslip was moved by a piezoelectric stage and simultaneously tracked directly and recorded to video tape. Recording to SVHS video tape resulted in an increase in the mean radial error as well as an increase in the standard deviation relative to direct tracking (figure 4); 1.9 nm versus 1.4 nm mean radial error, respectively.

*Compression effects.* When tracking, images are often saved to the hard drive. In order to save space, digital compression algorithms are used. Unless a compression algorithm is lossless (all pixel values are preserved exactly as in the original uncompressed image as in PNG and ZIP) there will be artifacts resulting from compression (JPEG, MPEG, most other methods). These artifacts add an additional noise component; can this component affect the accuracy and precision of a tracking algorithm? To examine this, a stack of images was compressed with various algorithms and tracked using each tracking method.

From this study, we discovered that for simulated fluorescence and DIC images with a reasonable level of noise (S/N ~14) the compression methods had little effect (figure 5) unless compression was aggressively applied (an exception being Cinepack, which did not work as well for our test images). Hence, it seems likely that in real-world conditions, positional errors introduced by image compression would be small compared to the deviations introduced by photon shot noise. An additional caveat is that compression algorithms that reduce the number of gray levels (such as the 'video' format under QuickTime) will artificially limit the accuracy tracking algorithms can achieve. Methods of compression that require color should be avoided by people using grayscale cameras, as color representations of grayscale

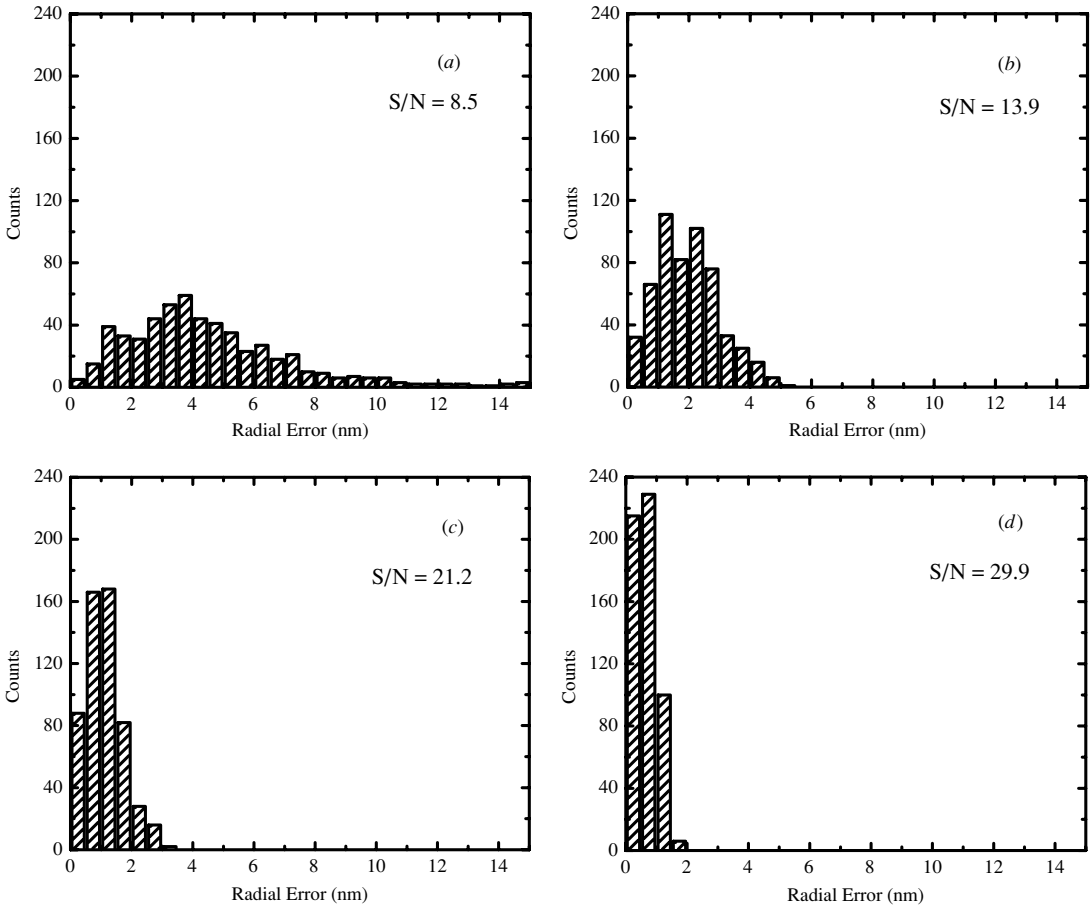


**Figure 3.** As S/N changes, so does the distribution of radial errors. At an S/N of 8.5 (*a*) the radial error shows the greatest spread. As S/N increases, this distribution becomes tighter (13.9 (b), 21.2 (c), 29.9 (d)) but never reaches zero (even at infinite S/N, data not shown). The standard deviation is typically half the mean value. All images had 33 nm/pixel and were tracked using LabVIEW Para. The distribution is representative of the other methods at the same S/N.

**Table 1.** Compression ratio resulting from applying the different compression methods to a stack of simulated fluorescent images (550 images, S/N 13.9).

| Compression type | Compression ratio |
|---|---|
| JPEG 1000 | 1.7:1 |
| JPEG 900 | 4.3:1 |
| JPEG 800 | 8.9:1 |
| JPEG 700 | 13.8:1 |
| JPEG 600 | 19.9:1 |
| JPEG 500 | 28.2:1 |
| JPEG 400 | 30.6:1 |
| PNG | 1.5:1 |
| MPEG 4 | 14.3:1 |
| Sorenson 3 best | 1.7:1 |
| Sorenson 3 high | 2.5:1 |
| Motion JPEG-A best | 1.4:1 |
| Motion JPEG-A high | 2.9:1 |
| QuickTime video | 2.0:1 |
| Cinepack | 3.4:1 |
| Indeo | 2.2:1 |
| Zip | 1.6:1 |

take up a great deal of space (typically, three times the space). Table 1 summarizes some of the compression methods with the compression ratios measured during our testing (mean of 550 images compared to a stack of TIFF images). During the compression trials, a weakness in MetaThresh1 was revealed: in a few cases, the automatic threshold level resulted in the program failing to track or performing an unusually bad track. MetaThresh2, which uses a manually set threshold, had no difficulties.

*Microscopy: fluorescence versus DIC*

While fluorescence microscopy uses the sample fluorescence to create contrast, DIC microscopy relies on changes in the index of refraction in the sample to generate contrasted images. Qualitatively, three differences stand out for DIC and fluorescence images. First, fluorescence images (of beads, virus particles, etc.) typically have a very circular appearance similar to that in figure 1, while DIC images often have a dark side and a light side destroying any radial symmetry the underlying object (a bead, for instance) may have (see insert in figure 6). Second, fluorescent objects are usually bright on a very dark background while DIC images are typically darker and lighter than a fairly high background value (relative to fluorescence images). Third, DIC images

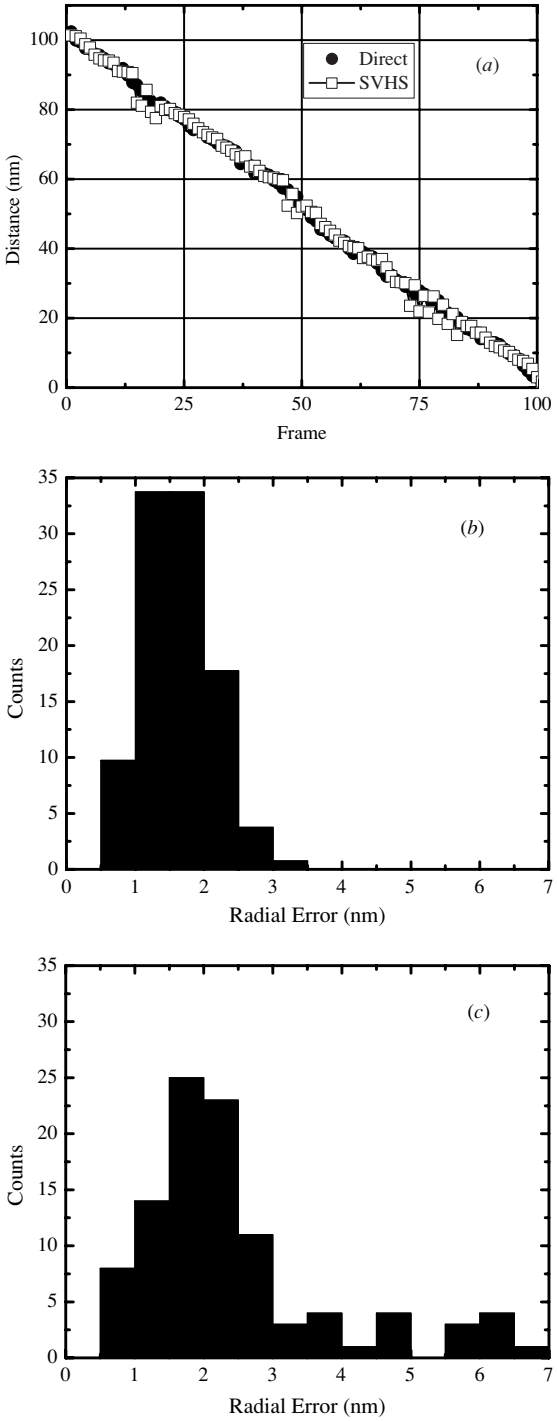


**Figure 4.** Effects of cassette tapes on tracking accuracy. (*a*) Tracking from SVHS video tapes reduces the accuracy by about 0.5 nm with respect to direct tracking from a 30 nm/pixel camera, resulting in a more noisy track. In the distribution of radial errors for direct tracking (*b*) and SVHS tracking (*c*) a longer tail is observed for tracking done from SVHS. SVHS appears smoother than VHS in general (data not shown).

of radially symmetric objects are often not radially symmetric but do have an axis of symmetry that is not always aligned with the *x* or *y* axes of the camera system.

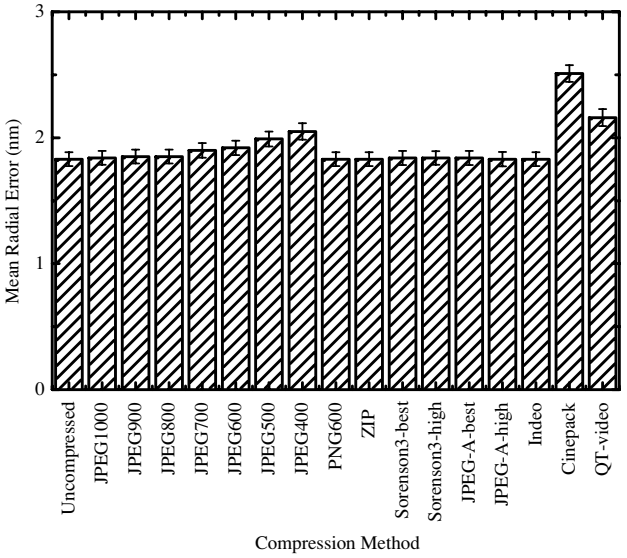


**Figure 5.** The accuracy of the tracking method for different image compression formats. Only Cinepack showed a large change compared to the uncompressed result. All other stacks were generated by compressing/decompressing the stack used to obtain the results for the 'unknown' column. The image stack was made from a data set at 33 nm/pixel, S/N of 13.9. Error bars represent SEM for 550 measurements.

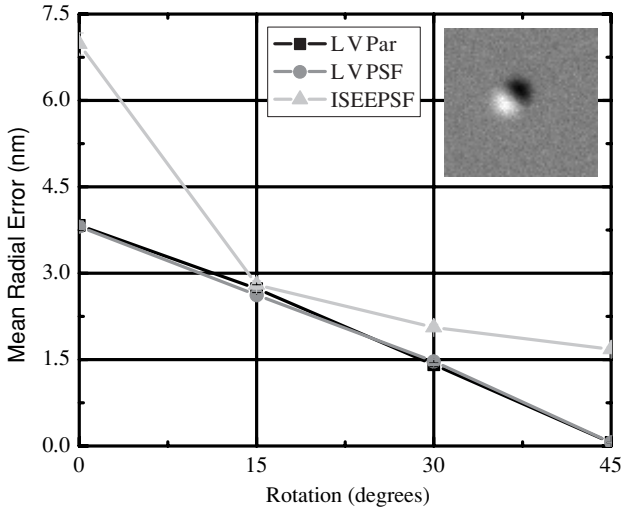


**Figure 6.** Rotation of DIC image versus mean radial error for the parabolic methods. Notice how the error falls almost linearly with rotation aligning the axis of symmetry with the *x* axis. Error bars represent the SEM and are smaller than the symbols. The inset shows an un-rotated simulated DIC image of a bead.

In the simulations, pseudo-DIC images are slightly harder to track than fluorescence images. Results for pure centroid and correlation/centroid methods are not affected by the axis of symmetry not being aligned with the *x* or *y* axes of the camera system, but methods that make use of correlation/parabolic or correlation/parabolic surface fitting are strongly affected by rotation of the axis of symmetry (figure 6). In the case of these pseudo-DIC images, the correlation image is elliptical and the long axis of the ellipse is

aligned along the symmetry axis in the image. The reason the parabolic methods fail is clear on inspection of the equations which are fit in each case (see materials and methods). The equations are oriented to lie along the *x*–*y* axes. In theory, performance of these algorithms can be improved significantly by allowing the parabolic equation to rotate or by rotating the image so the axis of symmetry coincides with either the *x* or *y* axis.

For real DIC images we made the following qualitative observations. When using LV-PSF with an odd grid size for parabolic fitting, very clear jumps appeared halfway through each pixel while with an even grid size these jumps did not appear. This jumping did not appear with either odd or even grid size for simulated fluorescence images. We believe the reason an even grid does better is because it lacks a clear center point. Despite the jumps, the mean radial error did not suffer much degradation. Meta-TM and Meta-Thres1 did not track the sample DIC images well, displaying pixel latching ( jumping between whole pixel values). Generally, DIC images require more care in setting the parameters of the tracking algorithm (template/search region size, threshold level and grid size where applicable) than tracking of fluorescence images. The pattern of pixel bias is clearer for tracks of DIC than for simulated fluorescence, but tend to follow the pattern reported by Cheezum *et al* (sine or triangle wave-like). Settings for template size and search radius must be carefully explored to avoid producing steps in ISee PSF, ISEE CM and LVCM.

*Microscopy: magnification effects*

The actual relationship between a pixel in the image and the corresponding number of nanometers in the object (and hence the 'total magnification' of the image) depends on both the physical size of the pixels on the camera's CCD chip and the optical magnification of a microscope. As magnification decreases, the same object will appear smaller. This can have two effects on tracking algorithms. First, fewer pixels are available to average to produce a measurement of the mean, resulting in a wider possible spread. Second, tracking algorithms are capable of detecting only fractional pixel changes of a certain size regardless of how many nanometers a pixel represents. In principle, this results in a linear loss of accuracy with lower magnification if the S/N is unaltered. But is this what we observe experimentally?

Indeed, best accuracy results from using the highest magnification available, being sensitive to issues of S/N. The mean radial error does change essentially linearly with magnification (figure 11). Thus, 4× more magnification means 4× improved accuracy. The SEM (or SD) also scales essentially linearly with magnification, although it is hard to see in the figure. However, as the magnification increases, the illumination will decrease as the square of the magnification [26] (see page 127, 137) resulting in a decrease in S/N proportional to magnification if the overall illumination is not increased externally. With the reduced S/N (more noise), the accuracy of the tracking algorithms falls off as demonstrated in figure 2. Thus, there is a practical limit to the maximum magnification one can achieve; in practice usually 30–40 nm/pixel. However, not all methods are equally affected by noise: methods based on pure centroid are more sensitive to noise than correlation-based methods. If a threshold is not applied, or if the threshold fails to isolate the object from the noise, then the noise-related impairment of the pure centroid methods becomes dramatic (see LVCent in figure 2).

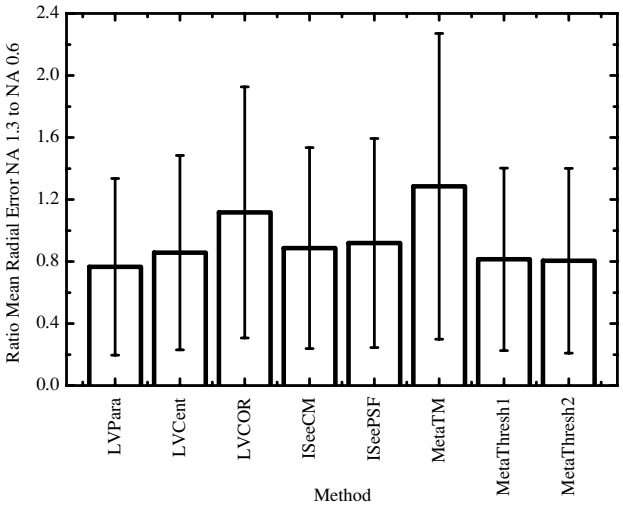


**Figure 7.** Ratio of mean radial error at NA 1.3 to the mean radial error at NA 0.6 for the different methods at a magnification of 33 nm/pixel and S/N of 13.9. While small deviations about 1 are visible in particular methods here, they are not reproduced at other magnifications and so are not meaningful. Error bars represent standard deviation.

*Microscopy: numerical aperture effects*

Another factor that changes the image of an object is the numerical aperture (NA) of the objective used.

Figure 7 shows the effect of NA on the relative mean radial error for all methods at a magnification of 33 nm/pixel. A value of 1 means that the mean radial error was the same for NA 1.3 and NA 0.6. A value near 1 was typical, and the deviations above or below 1 for the different methods visible in this graph should not be interpreted as a trend as the pattern does not hold for other magnifications. Thus, it appears that overall NA is not important. Note however, that for clean comparisons of the importance of NA, in our synthetic images, changes in NA were independent of signal-to-noise. Thus, when the numerical aperture changed, the S/N did not. In cases where light is limiting, S/N will potentially decrease as NA decreases and S/N is known to affect accuracy (figure 2).

*A priori*, it was unclear what to expect from changes in numerical aperture: resolution (i.e. ability to differentiate between close objects) improves with high NA, which might suggest that the accuracy of particle position determination might also improve with high NA. However, a lower NA results in a wider point-spread function, meaning that at the same magnification an object will appear larger. Thus, in principle as the object extends over more pixels, one might have more data to fit to, which might improve accuracy. These

competing effects appear to balance out, as we found no effect of NA on accuracy. However, in a real experiment, we expect that lowering the NA while holding the magnification constant could decrease tracking accuracy due to a decrease in the S/N ratio. The illumination of the CCD scales with the square of the numerical aperture [26] (see page 137). If one used the same magnification lens but with the NA values tested here the higher NA lens would provide $1.3^2/0.6^2 = 4.7$ times the illumination. Since the shot noise of the system goes as the square root of the illumination, the S/N will be equal to the square root of the illumination. So for our example, the S/N for NA 1.3 will be about $\sqrt{4.7} \approx 2$ times higher than for NA 0.6, provided the illumination is not adjusted by other means. If it is possible to avoid a decrease in S/N (e.g. by increasing illumination) or if the S/N is already high (greater than about 30) then the NA should be irrelevant as far a tracking accuracy is concerned.

*Digital versus analog cameras*

Analog images are actually the composite of two exposures, one for the odd lines the other for the even, taken 1/60th of a second apart and combined (interlaced) 30 times per second, for the NTSC standard, to produce an image. For fast moving objects, this creates a distinct serrated appearance on the border of objects because the object has shifted between frames. Progressive scan digital cameras do not do this; they instead take 30 whole images every second. Analog interlacing could thus be expected to result in an increased error in determining the position of the object being tracked.

To test the effect of interlacing, beads stuck to a microscope coverslip and moved by a piezoelectric stage were imaged using both digital and analog cameras. Necessarily, their magnifications were different: 24.3 nm/pixel for the digital camera versus 30 nm/pixel for the analog camera. The values compared in the following are adjusted to account for this magnification difference. For slow motion along the $x$-axis (30 nm $s^{-1}$) the relative errors were as follows: 1.4 nm for the digital camera versus 1.4 nm for direct tracking of analog camera data (tracking off a SVHS record increased the error as discussed above). Similarly, for fast motion (1 $\mu$m $s^{-1}$) the errors were 2.2 nm in both cases, suggesting that interlacing does not affect the accuracy of particle tracking while intuitively one would expect it to.

To further investigate the effect of interlacing, the program generating the pseudo-DIC images was altered to create noise-free simulated analog images: the object was moved twice per whole frame and alternating lines from each half frame were interlaced. Multiple sets of data were created to simulate slow and fast object displacement: from a small fraction of a pixel/frame to about 3 pixels/frame. This corresponds to a velocity range of 6–96 nm/frame, the pixel-size being 33 nm in this simulation. These noise-free images revealed no distinct effect resulting from their analog nature. Although the mean radial error and SD values varied, it was in no pattern (figure 8). Moreover, adding noise masked any observed variation for the two cases tested of 2/11 and 10/11 of a pixel displacement per frame.

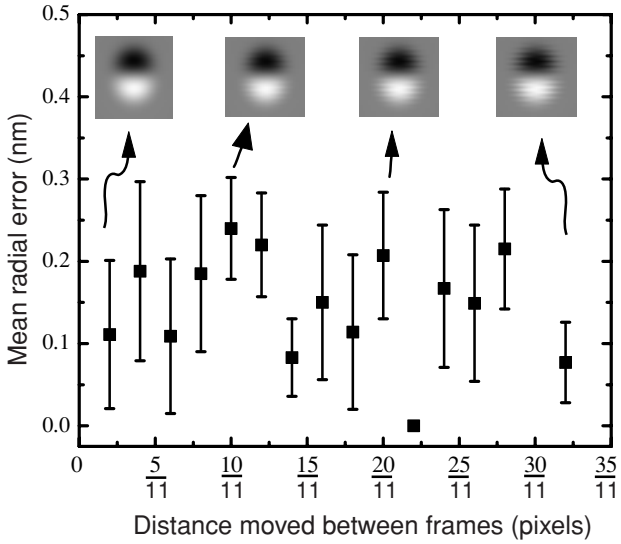


**Figure 8.** Mean radial error versus fractional pixel movement between frames. Error bars are standard deviation. Inset shows (from left to right) the appearance of the 2/11, 10/11, 20/11 and 32/11 objects.

We also performed a qualitative comparison of video tracking and quadrant photodiode tracking, a method known to have nanometer accuracy. In quadrant photodiode-based tracking, laser light scattered off the moving particle is detected by a segmented photodiode; changes in the difference signals between the different quadrants reflect changes in the position of the particle [27]. While the quadrant photodiode is fast, its nonlinear response outside a small region makes it unsuitable for measurements of large-scale motions (e.g molecular motor processivity). This system also has a disadvantage *in vivo* where objects outside the plane of focus interfere with the laser used for position detection. Video tracking methods were found to follow the quadrant photodiode track relatively well, despite their lower temporal resolution (figure 9). This alignment indicates similar precision is possible from video tracking as from the quadrant photodiode, though video suffers from its slow speed and from unavoidable pixel bias [21]. Quick events, such as a molecular motor's step, are more easily seen in quadrant photodiode data. A fast camera system (currently easily attainable with digital cameras) and custom or off-the-shelf video tracking software, however, should be able to give excellent results in situations where the quadrant photodiode would be unusable.

*Method bias and other errors*

One subtlety when tracking is the (user-defined) choice of template size. This was found to have a dramatic effect on most tracking methods. In figure 10, steps that do not exist in the raw data are observed as the template size rises. A similar trend is generally observed for all other methods tested except for LVPara and LVPSF which only look at the brightest pixel and its nearest neighbors in the correlation image. This artificial step generation is probably linked to the auto threshold function failing to choose a good threshold

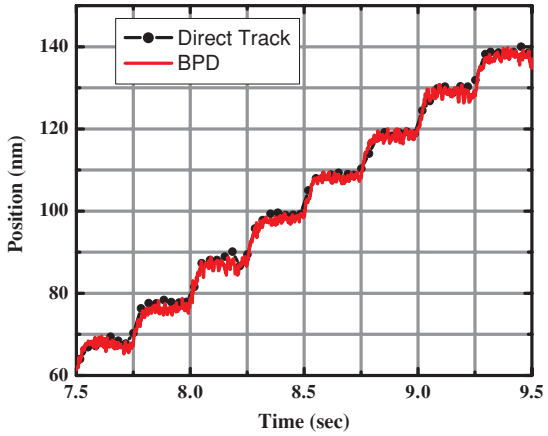


**Figure 9.** The precision of video tracking (black) is compared to a quadrant photodiode track (red) of a bead moved on a piezo stage in 10 nm steps. As described in the main text of this paper, the photodiode, while being very precise, has a linear response only over small distances (∼150 nm) which makes it unusable when objects are moving long distances. Video tracking is shown here to give comparable precision but with a much smaller temporal resolution. The BPD record was median filtered.

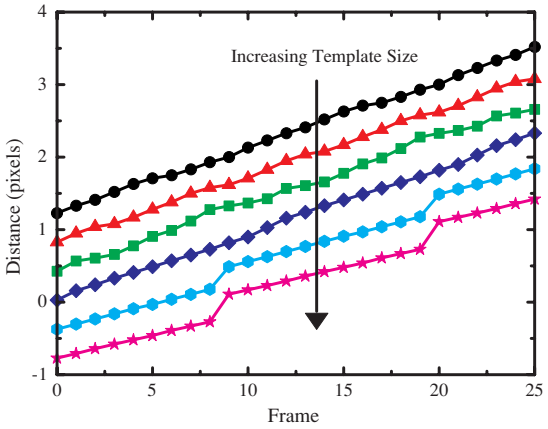


**Figure 10.** ISee-CM tracks at different template sizes (tracks offset for clarity). Note that at larger sizes a non-existent step is observed. These results are for a no-noise image stack. Template size, from top to bottom: 22, 26, 30, 40, 50, 60 pixels.

value. Changing the search region size or manually setting the threshold or changing the properties of the auto threshold function can counteract this effect. Much of the same holds for noisy conditions (data not shown).

## *Discussion*

*Doing the best to follow the object* Most tracking methods investigated do reasonably well, with the results typically clustering around a few nanometers of mean radial deviation from the true position. Thus, the typical claim of 10 nm accuracy is conservative as long as the measurements are made with high enough magnification that each pixel is 40 nm in size or less and S/N is kept above 10. ISee's NanoTrack method is particularly good (though not as good as other methods in situations of almost no noise) as it has consistent performance over a wide range of S/N. Metamorph can also yield good results using the MetaThresh2 option, but in this case more user expertise is required to appropriately set the threshold level (as discussed below). Good results are possible with pure centroid methods but this requires special attention to the threshold level, and becomes limited more quickly by S/N (see below). That being said, pure centroid methods are attractive because, being computationally simple, they allow higher speed.

*Caveats and subtleties* In correlation-based methods, a large template with a small search region can cause serious problems. In some cases, the correlation image may become filled by the correlation object (see supplementary figure II available from stacks.iop.org/PhysBio/2/60). When the correlation object is allowed to overfill the correlation image in this way, information important for the center-of-mass calculation is lost and errors (apparent steps where no steps are actually present, figure 10) will occur. This is most likely to occur when the template image is very large in relation to the search region. In such cases it is possible to manually set a threshold level that will provide better results, or alter the settings for the auto-thresholding function. Threshold Image is the best method in MetaMorph, although careful attention must be paid to setting the threshold level. Best results were obtained by increasing the threshold level until as much of the background was lost as possible while retaining the shape of the object (supplementary figure III available from stacks.iop.org/PhysBio/2/60). Using the automatic thresholding setting in MetaMorph, 'threshold for light objects', similar results were often obtained. However, this method occasionally tracked poorly or failed to track.

Conversely, the correlation object may become smaller than the grid chosen for parabolic surface fit methods. When this happens an analogous effect occurs—the trace of particle motion displays steps. This creates a lower limit on the magnification, as the object must be large enough to ensure the correlation image of the object is larger than the desired grid size.

*Magnification, numerical aperture and illumination* As previously mentioned, illumination scales as the square of NA and the inverse square of magnification [26] resulting in the S/N scaling with NA and inversely scaling with magnification (provided noise is in the form of shot noise). What sort of differences in S/N can be expected in typical situations? As an example let us compare the S/N of both a 60× air objective having a NA of 0.85 and a 100× oil objective having a NA of 1.4 to a 60× oil immersion objective having a NA of 1.4. Assuming that the illumination is only changed by the choice of the objective and taking a typical S/N of 15 for the 60× oil images one can use equation (4) to calculate the S/N (SN) of an image relative to that obtained by the 60× oil objective (SN):

$$\frac{\mathrm{NA}'}{\mathrm{Mag}'} \Big/ \frac{\mathrm{NA}}{\mathrm{Mag}} = \frac{\mathrm{SN}'}{\mathrm{SN}} \tag{4}$$

where NA is the numerical aperture, Mag is the magnification, SN is the signal-to-noise ratio and primed values are those of

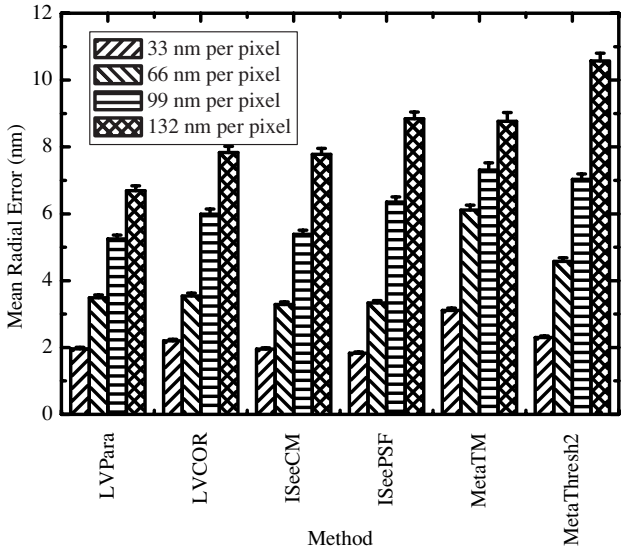


**Figure 11.** Mean radial error versus magnification for different tracking methods. The mean radial error scales with magnification. On average, four times more magnification means four times more accuracy. Error bars represent SEM for 550 measurements.

the objective being investigated. For the lenses and values chosen above, the S/N would become about 9 for both the 60× air lens and the 100× oil lens. Thus, in this case, the 60× air and the 100× oil would have the same performance as far as the S/N is concerned. The 100× lens, however, will still have an advantage due to the scaling of tracking resolution with magnification (figure 11).

*Use of the tracking data for velocity measurements and co-localization studies* In this manuscript, we evaluated the accuracy of a number of particle tracking methods. In most cases, we found a mean radial error significantly less than 5 nm. From a typical histogram of radial errors (figure 3), we also observe that any *individual* measurement is likely to be within approximately 5 radial nm of its actual position for images with typical S/N values. This magnitude of individual variation has implications for two uses of such position data: calculation of instantaneous velocities, and measurements of particle co-localization using two fluorescence channels to look at two classes of different fluorescently labeled particles.

Measuring a particle's instantaneous velocity should be done with care. For the case shown in figure 3(*b*), a particle moving 1 nm between consecutive frames could be measured to have moved as much as 10 nm (5 nm uncertainty for both endpoints, in opposite directions) and its instantaneous velocity would therefore be measured to be ten times larger than the actual value. As the histogram shows, however, an error that large is very unlikely, and the measurement in the following frame is likely to be closer to the true value. After a certain number of frames—depending on the speed of the particle—even in the worst-case scenario this uncertainty in position determination will contribute only a small percentage of the total displacement. Hence, the number of frames used to calculate the 'instantaneous' velocity should be chosen dependent on the approximate mean velocity of the particle. This should be done in a way that, on average, from the start to end of the chosen period the particle will have moved a few multiples of the maximal error. For instance, for a particle moving 100 nm $s^{-1}$, if the period is chosen to be 0.33 s, on average the particle will have gone 33 nm, so a typical 'bad' error of 6–8 nm (3–4 nm from each endpoint) would give approximately a 20% error in calculation of instantaneous velocity. For slow moving particles, it is possible to average the position from immediately successive points to decrease the position error.

A closely related issue is the co-localization of different fluorescently labeled objects. A similar argument leads us to the conclusion that two objects can be found to be separated by as much as 10 nm (5 nm uncertainty for each) while they in reality lie on top of each other. This, however, can be improved if the co-localization of many similar objects is measured. The uncertainty will then be close to about 6 nm (two times the peak position in the histogram). This, however, is only true for extended objects. If, on the other hand, the two objects are labeled with single fluorophores, a Gaussian fit to the respective intensities should be able to localize them with higher accuracy [14–16, 21].

Additionally, the noise inherent in the system can cause apparent sub-diffusion, discussed in detail by Martin *et al* [28].

## Conclusion and outlook

Particle tracking is powerful, and can be done with remarkable accuracy when one pays attention to a few details. With a good signal-to-noise ratio and large magnification, without undue work it should be possible for most labs to achieve better than 5 nm accuracy in localization of individual particles. It is similarly easy, however, to reach false conclusions when tracking by underestimating the effects of the different factors affecting accuracy discussed in this paper. Hence, utmost care must be taken. Given the numerous new ways of visualizing proteins and the increased attention being paid to dynamic cellular organization, the use and importance of such tracking data should increase dramatically in the years to come.

## Acknowledgments

We are especially grateful both to R Mallik for numerous discussions as well as comments on the manuscript, and to Dmitri Petrov for his help in implementing the simulated DIC program. B Carter was supported by a training grant from NIGMS, and G T Shubeita was partly supported by fellowship from the Helen Hay Whitney foundation. This work was supported by NIGMS grant GM-64624-01 to SPG. Correspondence and requests for materials should be addressed to Steven P Gross. (email sgross@uci.edu). Free tracking software can be downloaded from the Gross Lab website, current address: http://bioweb.bio.uci.edu/sgross. As a condition of use of this software, it must be acknowledged in the resulting manuscripts, and this manuscript be cited.

## Glossary

*Accuracy.* In this paper, the uncertainty with which a method determines the position of an isolated object.

*Correlation (COR).* Measure of how related a region of an image is to a template.

*Interpolation.* A mathematical method that estimates the value of a function at points between given values.

*Lossy.* A method that loses information in the process of compression.

*Pixel bias error.* The tendency of a tracking method to prefer certain regions in a pixel.

*Signal-to-noise ratio (S/N).* The ratio between the number of signal photoelectrons to the number of noise photoelectrons (produced by electronic noise, etc.) received.

*Sum-absolute difference (SAD).* A method that determines the amount of translation of a template relative to an image by minimizing the sum of absolute differences.

## References


[1] Nybakken K and Perrimon N 2002 Hedgehog signal transduction: recent findings *Curr. Opin. Genet. Dev.* **12** 503–11

[2] Schnapp B J 2003 Trafficking of signaling modules by kinesin motors *J. Cell Sci.* **116** 2125–35

[3] Kholodenko B N 2003 Four-dimensional organization of protein kinase signaling cascades: the roles of diffusion, endocytosis and molecular motors *J. Exp. Biol.* **206** 2073–82

[4] Corcoran L J, Mitchison T J and Liu Q A 2004 novel action of histone deacetylase inhibitors in a protein aggresome disease model *Curr. Biol.* **14** 488–92

[5] Gunawardena S and Goldstein L S 2004 Cargo-carrying motor vehicles on the neuronal highway: transport pathways and neurodegenerative disease *J. Neurobiol.* **58** 258–71

[6] Catlett N L and Weisman L S 2000 Divide and multiply: organelle partitioning in yeast *Curr. Opin. Cell. Biol.* **12** 509–16

[7] Kopito R R 2000 Aggresomes, inclusion bodies and protein aggregation *Trends Cell Biol.* **10** 524–30

[8] Hachiya N S, Watanabe K, Yamada M, Sakasegawa Y and Kaneko K 2004 Anterograde and retrograde intracellular trafficking of fluorescent cellular prion protein *Biochem. Biophys. Res. Commun.* **315** 802–7

[9] Ghosh R N and Webb W W 1994 Automated detection and tracking of individual and clustered cell surface low density lipoprotein receptor molecules *Biophys. J.* **66** 1301–18

[10] Gelles J, Schnapp B J and Sheetz M P 1988 Tracking kinesin-driven movements with nanometre-scale precision *Nature* **331** 450–3

[11] Mallik R, Carter B C, Lex S A, King S J and Gross S P 2004 Cytoplasmic dynein functions as a gear in response to load *Nature* **427** 649–52

[12] Work S S and Warshaw DM 1992 Computer-assisted tracking of actin filament motility *Anal. Biochem.* **202** 275–85

[13] Lee G M, Ishihara A and Jacobson K A 1991 Direct observation of brownian motion of lipids in a membrane *Proc. Natl. Acad. Sci. USA* **88** 6274–8

[14] Anderson C M, Georgiou G N, Morrison I E, Stevenson G V and Cherry R J 1992 Tracking of cell surface receptors by fluorescence digital imaging microscopy using a charge-coupled device camera. Low-density lipoprotein and influenza virus receptor mobility at 4 degrees C *J. Cell Sci.* **101** 415–25

[15] Schutz G J, Schindler H and Schmidt T 1997 Single-molecule microscopy on model membranes reveals anomalous diffusion *Biophys. J.* **73** 1073–80

[16] Yildiz A, Forkey J N, McKinney SA, Ha T, Goldman Y E and Selvin PR 2003 Myosin V walks hand-over-hand: single fluorophore imaging with 1.5-nm localization *Science* **300** 2061–5

[17] Yildiz A, Tomishige M, Vale RD and Selvin P R 2004 Kinesin walks hand-over-hand *Science* **303** 676–8

[18] Kagawa Y and Tsuchiya Y 2003 Stepping motion of the organelle in a perfused characean cell *FEBS Lett.* **546** 209–12

[19] Faivre-Moskalenko C and Dogterom M 2002 Dynamics of microtubule asters in microfabricated chambers: the role of catastrophes *Proc. Natl Acad. Sci. USA* **99** 16788–93

[20] Bohs L N, Friemel B H, McDermott B A and Trahey G E 1993 A real time system for quantifying and displaying two-dimensional velocities using ultrasound *Ultrasound Med. Biol.* **19** 751–61

[21] Cheezum M K, Walker W F and Guilford W H 2001 Quantitative comparison of algorithms for tracking single fluorescent particles *Biophys. J.* **81** 2378–88

[22] Gross S P, Tuma M C, Deacon S W, Serpinskaya A S, Reilein A R and Gelfand V I 2002 Interactions and regulation of molecular motors in Xenopus melanophores *J. Cell. Biol.* **156** 855–65

[23] Young D, Glasbey C A, Gray A J and Martin N J 1998 Towards automatic cell identification in DIC microscopy *J. Microsc.* **192** 186–93

[24] Simonetti JH 2004 Measuring the signal to noise ratio S/N of the CCD image of a star or nebula. http://www.phys.vt.edu/~jhs/phys3154/snr20040108.pdf; 2004

[25] Gain. Photometrics (Available online at http://www.photomet.com/library_enc_gain.shtml)

[26] Inoue S and Spring KR 1997 *Video Microscopy: The Fundamentals* 2nd edn (New York: Plenum)

[27] Visscher K and Block S M 1998 Versatile optical traps with feedback control *Methods Enzymol.* **298** 460–89

[28] Martin D S, Forstner M B and Kas J A 2002 Apparent subdiffusion inherent to single particle tracking *Biophys. J.* **83** 2109–17